Proceedings Kenya Geothermal Congress 2024.
Nairobi, Kenya, 16 – 18, July, 2024.

Reproducing the Late Miocene Sandstone Porosity using 3D Printing for Laboratory Geothermal Reinjection Experiments: Successes, Challenges, and Future Directions

Rita Mwendia Njeru[1], Akhmad Sofyan [1], Zsolt Geretovszky[2], Balázs Kóbor[3], Tamás Medgyes[3] Matthias Halisch[4], János Szanyi[1]

[1]Department of Mineralogy, Geochemistry and Petrology, Faculty of Earth Science, University of Szeged, 13 Dugonics Square Szeged 6720, Hungary

[2]Department of Optics and Quantum Electronics, University of Szeged, Dóm Sq. 9, 6720, Szeged, Hungary

[3]Geothermal Energy Applied Research Center, University of Szeged (GEAR)

[4]Leibniz Institute for Applied Geophysics (LIAG), Dept. 5 - Petrophysics & Borehole Geophysics, Stilleweg 2, D-30655 Hannover, Germany

Keywords

3D printing, geothermal energy, Late Miocene sandstone, micro-CT imaging, sandstone porosity, selective laser melting (SLM).

ABSTRACT

This research pioneers the replication of Late Miocene sandstone porosity via 3D printing, emphasizing its application in geothermal energy experiments. Our objective was to recreate the porosity of Late Miocene sandstone accurately using selective laser melting (SLM) and evaluate its effectiveness through comparison with original model from micro-CT imaging. We compared porosity across natural, digitally modelled, and 3D-printed sandstone samples. Results indicated that 3D printing slightly alters porosity, primarily due to the presence of support materials resulting from the printing process. The study highlights the need for enhanced printing materials, refined post-processing methods, and printers with higher resolution to improve porosity replication accuracy. Our findings also suggest considering alternative methods of manufacturing artificial Late Miocene sandstone like sand compaction with calcium carbonate cement to broaden the artificial samples applicability in lab experiments, thereby enriching our understanding of geothermal systems. This investigation not only advances the field of geothermal research through 3D printing of Late Miocene sandstone but also sets the stage for future studies focused on replicating geological structures for sustainable energy exploration.

1. INTRODUCTION

Unlike other natural energies like coal, oil, gas, and minerals, geothermal energy cannot be transported and can only be used for production development (Byrtus et al., 2022). Geothermal energy can only be generated at certain times, needs to be reserved, and is not available everywhere (Angumba et al., 2022). However, geothermal energy is a replenished source and can be utilized throughout the year (Zafar et al., 2021). Therefore, the potential of geothermal energy needs to be investigated and discovered (Harrouz et al., 2018).

Along with the increase in energy consumption and needs due to changes in population growth and lifestyle (Esmaeili Shayan et al., 2021), the production of geothermal energy as alternative energy needs to be increased to meet national energy targets. Geothermal energy provides opportunities to meet the energy needs of future generations (Yudha, Tjahjono & Longhurst, 2022). Hungary has shown a significant increase in geothermal district heating over recent years, which is mainly due to two new large projects (Miskolc and Győr). Geothermal district-heating systems and thermal water heating cascade systems are available in 21 cities representing an installed capacity of approximately 210 MWth and an annual production of 350 GWhth/y. Individual space heating (mostly associated with spas) is available at 35 locations representing an estimated installed capacity of approximately 28 MWth and annual production of approximately 63 GWhth/y (Toth & Toth, 2020). In developing geothermal energy, several steps need to be carried out, including the preliminary 3G survey (geology, geochemistry, geophysics), exploration 3G survey, exploration drilling, project review and planning, field development, power plant construction, commissioning, and operation (Sofyan, 2024).

When geothermal energy is utilized, heat energy from the geothermal fluid that is released to the earth's surface is converted into electrical energy. (Sofyan, 2023). The fluid comes from the geothermal reservoir layer, which is created as a result of conduction and convection heat transfer from a heat source to its surroundings (Saptadji, 2001). In addition, the convection heat transfer describes the process by which heat moves from the geothermal fluid to the production casing, while conduction heat transfer refers to the movement of heat from the well casing to both the cement and the formation (Sofyan, 2023). In the broader context of reservoir evaluation, each layer within the earth's subsurface has unique characteristics, including varying fluid and rock compositions, as well as different levels of rock hardness. This diversity requires extensive research to identify the most effective methods to overcome challenges at specific reservoir locations (Gunnlaugsson et al., 2014).

Sandstone formation is a sedimentary rock used in the oil and gas industry, geothermal energy, building, and other sectors. Sandstone's porosity, or the existence of void inside the rock, is an important property that influences the characteristics and usages of the sandstone in various industries like geothermal energy (Jakus et al., 2018). Porosity affects rock permeability because it affects the flow of fluids such as geothermal fluids, oil, and gas through the rock (Lee & Heller, 1990). Consequently, proper porosity assessment is essential for estimating reservoir productivity and improving recovery methods (Emanuel et al., 1989).

Recent advances in micro-CT scanning and 3D printing have opened up new avenues to properly replicate sandstone porosity (Emanuel et al., 1989). Micro-CT scanning is a non-destructive imaging technology capable of producing high-resolution three-dimensional images of the interior structure of objects, including porous materials such as sandstone (James W. Jennings, 2002). In contrast, 3D printing is a manufacturing process capable of producing physical objects with complicated geometries, including porous structures (Emanuel et al., 1989). It may be possible to create precise 3D-printed copies of sandstone porosity by combining these two technologies.

Based on the research conducted by Foldez (2004), if a rock sample is properly prepared, drained, vacuumed out, and then saturated with liquid, its effective porosity can be determined by the CT

measurement since the effective pore space of the cells (which can be filled up with liquid or gas) can be measured in which the effective porosity of each cell can be quantified (Földes et al., 2004). Based on CT measurements, the internal structure of core samples, the geometry of framework constituents, the porosity type and pore size distribution, as well as fracturing, can be described (Wu et al., 2022; Zhang, 2018).

According to Ishutov (2015), the combination of X-ray computed microtomography, digital pore network modeling, and 3D printing technology can transfer digital rock models into tangible samples that can be manufactured in various materials (Ishutov et al., 2015). Another research accomplished by Gomez (2019) investigated the mechanical behavior and permeability of 3D-printed sandstone analogs under triaxial conditions and found that the use of silica sand as the printing material has enabled the manufacture of specimens with a more rock-like porous structure (Gomez et al., 2019). These studies demonstrate the potential of 3D printing from micro-CT data to accurately reproduce the porosity of sandstone and provide tangible samples for further analysis.

Replicating sandstone porosity by 3D printing using micro-CT data is an exciting field of research that is currently in its early phases. Although 3D printing has been quite successful in recreating porosity, there are still many obstacles and limitations that must be overcome such as obtaining large samples with high resolution to properly replicate the sandstone at its original scale. In recent advances, Li (2021) successfully utilized two-photon polymerization 3D printing technology to replicate the true pore-scale structure of Berea sandstone, demonstrating the potential of high-resolution 3D printing in geosciences (Li et al., 2021). However, their approach produced only 500 μm samples which were unusable for laboratory investigations. Our study innovates on this concept by exploring the effects and implications of significant upscaling in 3D printing, specifically by 100 times the original size of the sandstone structure. This methodological shift is designed to provide new insights into the accuracy and application of 3D-printed rock proxies, particularly for large-scale geothermal reservoir simulations, and laboratory experiments. Future research should concentrate on improving 3D printer accuracy and resolution, developing new 3D printing materials and techniques to aid in the proper cleaning of the support materials used to support overhanging parts of the 3D printed rocks during printing, and investigating the mechanical and permeability properties of 3D printed sandstone analogs (Wu et al., 2022). Therefore in this study, we investigate how the best steel can be used to reproduce sandstone porosity of the Late Miocene sandstone.

This research significantly advances the field of 3D printing to replicate sandstone porosity by introducing a novel methodology involving a considerable 100-fold upscaling of the original sandstone structure. While existing literature extensively explores the application of 3D printing in geoscience and engineering, our innovative approach specifically addresses the challenge of achieving large and high-resolution samples, thereby enabling a more accurate replication of sandstone at its original scale. In contrast to prior studies, our focus on upscaling is geared toward practical applications in large-scale geothermal reservoir simulations and laboratory experiments. Our study builds on the foundation laid by Foldez (2004), Ishutov (2015), and Gomez (2019), integrating their insights into a comprehensive methodology. Notably, our research introduces a departure from existing studies by utilizing two-photon polymerization 3D printing technology and exploring the use of steel as a printing material. This research is also different from research conducted by Li's (2021) who replicated the true pore-scale structure of Berea sandstone using two-photon polymerization technology. The advances in this research showcase a significant departure from previous approaches, providing insights into the potential of high-resolution 3D printing in geosciences. This research offers a technological and scientific convergence that has the potential to expand our understanding of geothermal processes, contribute to sustainable energy generation, and solve real-world difficulties in the sector. It exemplifies the inventive spirit of scientific inquiry as well as its practical applications. While this research anticipates contributions to the field by providing artificial sandstone samples for laboratory investigations, potential cost efficiencies, and

advances in 3D printing technology, it is important to note that the specific impacts and cost reduction claims depend on further research and development. Existing literature supports the use of 3D printing in replicating sandstone porosity, but the extent of cost efficiency and widespread applicability in various fields is still a subject for exploration. The current research focuses on the methodology and findings within the scope of the Late Miocene sandstone replication, and any extrapolations to broader applications require further empirical support (Filinich & Chibey, 2020).

2. REVIEW OF SANDSTONE POROSITY AND 3D PRINTING ADVANCES

2.1. Sandstone Porosity

Sandstone, a sedimentary rock composed of sand-sized grains of mineral, rock, or organic material, exhibits varying levels of porosity. Porosity refers to the fraction of pore space in a rock volume expressed as a percentage. The Berea sandstone, for instance, exhibits a porosity range of 19% to 26% (Gomez et al., 2019). Experimental analysis of Upper Pannonian sandstones from the Hungarian Szentes Geothermal Field was performed to understand the formation properties affecting injectivity and productivity in these sandstone layers. Research on these sandstones showed varying levels of porosity, with certain samples showing porosity of up to 30% (Békési, 2022; Koroncz et al., 2022).

In both the geothermal and petroleum industries, there is a need for innovative technologies that can improve the economic viability of exploration and production. Understanding the geomechanical and transport properties of rocks is crucial for geoscience and engineering disciplines as they provide insights into how these properties respond to external stresses and subsurface flow regimes (Hodder et al., 2022).

According to Abutaha (2021), X-ray computed tomography (CT) can reveal the internal three-dimensional details of objects in a non-destructive way and provide high-resolution quantitative data in the form of CT numbers (Abutaha et al., 2021). The sensitivity of the CT number to changes in material density means that it can be used to identify lithological changes in cores of sedimentary rocks.

Porosity in sandstone can be characterized by several methods, including mercury intrusion porosimetry, nuclear magnetic resonance, and micro-CT (Siregar, 2020). Micro CT scanning has become a popular method for quantifying the porosity of rock samples due to its high resolution and non-destructive nature (Arandjelovic, 2015).

In the context of this study, micro-CT scanning was used to obtain high-resolution 3D images of the sandstone samples, which were then used to create a 3D-printed replica of the sample's porosity. The accuracy and quality of the 3D-printed replica were then compared to the original sandstone sample, as described in the following sections.

2.2. The 3D Printing Technology Advances

3D printing is a fabrication technique that constructs a three-dimensional object by depositing materials layer by layer, guided by a computer-generated design (Tamir et al., 2022). In the field of bioprinting, 3D printing has been used to create scaffolds for tissue engineering purposes (Qasim et al., 2019). Similarly in the petroleum industry, the application of 3D printing technology has facilitated the creation of sandstone replicas for investigating their mechanical behavior and permeability under triaxial conditions (Gomez et al., 2019).

Ishutov (2015) used 3D printing technology to create sandstone porosity models in their study (Ishutov et al., 2015). However, the resolution of the ZPrinter 650 3D printer used for this purpose was too poor (30 μm for pore space and 16 μm for grain matrix) to duplicate the Idaho Gray

Sandstone at its original scale. Therefore, upscaling was required. The procedure consisted of applying a binder material to a layer of sandstone powder and then curing the binder using UV light (Xie et al, 2021; Kim et al., 2019). This method produced strong sandstone models with substantial structures. These models were useful for studying the permeability properties of sandstone (Wang et al., 2022).

The difficulties in 3D printing sandstone models are various. One of the difficulties is getting the proper distribution of porosity and particle size of the sandstone analog. Researchers used sand powder and organic binder (Hodder et al., 2022), two-photon polymerization 3D printing technology (Li et al., 2021), and isotropic consolidated drained triaxial tests to accomplish this (Gomez et al., 2019). Another difficulty is getting the necessary resolution to properly replicate the sandstone at its original scale (Ishutov et al., 2015).

Researchers also experienced difficulties in post-processing and removing the support material used in the printing process without causing damage to the printed sample. Post-processing is essential to remove extra powder and binder material (Ishutov et al., 2015). The support material is difficult to remove and requires careful handling to prevent damage to the printed sample. Therefore, whenever possible, it is recommended that the support material be made easily removable without damaging the printed sample during removal. The scale of the printed models is also an issue because researchers have to print models of various sizes to explore the uniaxial compressive characteristics of rocks (Hodder et al., 2022; Wu et al., 2022).

Finally, using reconstructed image-processed CT scans, researchers must evaluate the correctness of the printed models by comparing them to the original sandstone (Almetwally & Jabbari, 2021). Despite these obstacles, 3D printing technology has demonstrated significant promise in replicating sandstone porosity and has been applied in a variety of disciplines, including geoscience and engineering, bioprinting, and the fashion industry (Abdallah et al., 2019).

3. SAMPLE MATERIAL & METHODOLOGY

3.1 Determination of Natural Sample Porosity

The sample studied in this research was a sandstone rock from the delta plain (Ujfalui Formation) in the Pannonian Basin. Because of its high porosity and permeability, this deposit is a viable resource for geothermal extraction in Hungary (Willems et al., 2021). The natural core sample was carefully sliced into a cylindrical shape with diameters of 33 mm (approximately 1.3 inches) and 40 mm (approximately 1.57 inches). Two methods were used to determine the porosity of the natural sample, namely the helium pycnometry method and the Archimedes-Triple weighing method.

First, the cut-out samples were dried to remove any moisture content. The helium pycnometry method was then used to determine the porosity of the sample. The measurement was carried out twice and the average value was taken.

The Archimedes (triple weighing) method was used as the second approach. The dry sample was weighed to get a dry mass value. Then, the sample was fully saturated with tap water with a density of 1 g/cm3, and then it was weighed to get a saturated mass value. The mass of the sample was measured once more with buoyancy. Each mass measurement was done three times, and the average value was calculated. The Archimedes equation 1 was used to calculate porosity.

$$Porosity = \left(1 - \frac{saturated\ mass - bouyant\ mass}{saturated\ mass - dry\ mass}\right) 100 \quad (1)$$

This equation allowed determining the porosity of the sample by considering the difference in mass between the saturated state, the buoyant state, and the dry state of the sample.

3.2. Digital Rock Porosity Determination (Micro-CT Imaging and Analysis)

The natural sample was further reduced to approximately 3 mm in size to allow for high-resolution imaging. The sample was imaged at a resolution of 1.15 μm. After that, the Avizo 2019 program was used to calculate the total and effective porosity of the resulting digital rock sample (Avizo, 2019).

To create a 3D printing model, the grains and voids in the digital sample were separated by applying the interactive thresholding module available in Avizo 2019 Software. It is crucial to note that the choice of the threshold value in this procedure is based on the investigator's discretion, which may result in some variation in the results across investigators. The result of this approach was a model that represented all grains. The model was cleaned to remove any tiny, disconnected grains caused by segmentation faults. Based on the study of the 500-voxel cube, this resulted in a linked grain cube model with a geometric size of 572.5 μm.

To create a mesh file, the resulting model was exported to the Dragonfly program, Version 4.1.0.647 for Windows, software from Object Research Systems (ORS) Inc., Montreal, Canada, accessible at http://theobjects.com/dragonfly. This mesh file was then exported in STL file format. This model was then sent to the 3D printer (Dragonfly software, 2021).

3.3 The 3D-Printing (Post-Processing and Quality Control) of the Artificial Sample

The 100-fold magnified replica of a cubic volume of the digital model was 3D printed. This magnification was chosen to guarantee that the voxel resolution of the printing process should match the geometric details of the sample, as resolved by its micro-CT measurements. Selective laser melting (SLM) was chosen and used to manufacture the sample from 316L stainless steel powder (nominal powder size distribution of 20-65 μm) on an EOS M290 metal printer (EOS GmbH). The choice of 316L stainless steel was influenced by logistical considerations in our lab setup. While differing from natural sandstone in mechanical and thermal properties, 316L stainless steel was the most feasible option available, balancing ideal requirements against practical availability.

Before printing the digital file was carefully checked to support printing that would ensure the least support material. However, no orientation was found that was able to fully achieve this goal, in which some supporting structures were printed and remained inside the printed sample, representing approximately 7% of the entire volume of the printed sample. In addition, the mixed/partially closed nature of the pore structure of the sandstone sample made it inevitable that some unused metal powder also remained inside the closed pores after printing. Therefore, the part was printed in the optimum orientation using a layer thickness of 40 μm, a hatch distance of 100 μm, a laser power of 214 W, and a scanning speed of 928 mm/s (equivalent to an energy density of 57.65 J/mm3) in a protective Argon atmosphere.

After printing, the sample underwent minimal post-processing, involving removal from the platform and milling off the support structure remnants. The use of 3D-printed models in our study reflects an effort to minimize environmental impact compared to extracting natural rock samples. Economically, it presents long-term benefits such as reduced fieldwork and consistent sample production. However, these advantages are balanced against the costs and sustainability of advanced 3D printing technologies, making it a crucial aspect in the evolution of geothermal research methodologies.

3.4. Porosity Measurements of the artificially manufactured sample

To determine the porosity of the artificial sample, Archimedes equation 2 was employed.

$$\varphi = \left(1 - \frac{\rho_{bulk}}{\rho_{skeletal}}\right) 100 \quad (2)$$

Here, ρ_bulk represents the bulk density of the sample, determined as the ratio of mass to volume. The mass of the sample was measured using a scale. The bulk density values were obtained through the application of three different methods, resulting in three distinct porosity values for comparison.

3.4.1 Volume determining by water displacement method

The volume of the sample was calculated by immersing the sample in a precisely measured quantity of water and measuring the volume of water displaced. To eliminate errors that could come from water entering the macropores of the sample, the sample was first sealed using vacuum sealing equipment. To improve accuracy, nine independent measurements were carried out, and the values of displaced water volume were averaged. Using this information, the bulk density (mass/volume) of the sample was calculated.

3.4.2 Volume calculations based on precise measurements of sample dimensions.

The dimensions of the sample were calculated by averaging 21 independent measurements using a pair of Vernier calipers with an error margin of 0.017 cm. The average volume was then calculated based on the measurements. Again the bulk density was determined from this method of volume determination.

3.4.3 Volume measurement using a 3D scanner

For this purpose, the SCAN in a BOX FX 3D scanner with IDEA 1.1 SR 8 FX software, available at Geochem Ltd., was used. This particular 3D scanner employs “structured light” technology. The sample was scanned from five different sides with a 72° rotation, including the top and bottom. Subsequently, the software generated a 3D digital model of the sample and computed the volume and surface parameters. This volume was used to calculate the sample’s bulk density.

3.5 The theoretical volume

According to the precision of the micro-CT scan, the digital model represented a cube of 500 voxels, with each voxel measuring 1.14551 µm. The volume of the simulated sample was properly determined using this information and then multiplied by an upscale factor of 100 for each side of the sample. This gave a theoretical volume of the printed sample.

In addition to the theoretical volume from the digital image, the laboratory determined volume values from the three laboratory methods used in which each method resulted in different bulk densities. Equation 2 was utilized to calculate the four porosity values of the sample according to the method used.

The skeletal density (ρ_skeletal) was obtained by calculating the average density of the sample composition, as defined in Equation 3.

$$\rho_{skeletal} = 7.77x_{metal} + 3.99x_{powder\ bed} + 6.9x_{support} \quad (3)$$

Here, $\boldsymbol{x_{metal}}$, $\boldsymbol{x_{powder\ bed}}$, and $\boldsymbol{x_{support}}$ represent fractional compositions of the pure metal part, the powder bed, and the support material of the sample, which were 90%, 3%, and 7% respectively as reported by the printing laboratory. It should be noted that $\boldsymbol{x_{metal}}+\boldsymbol{x_{powder\ bed}}+\boldsymbol{x_{support}}$ equals 1, indicating the combined density of the sample composition.

4. Results and discussion

4.1 Natural Sample Porosity

The porosity values of the natural samples through the Helium Pycnometry and Archimedes-Triple Weighing Methods were 28.1% and 27.74% (Table 1), respectively. These values served as a baseline for comparing the porosity values of the artificial samples. Helium pycnometry is known to provide very accurate results for total porosity, exceeding the accuracy achievable by other methods. Hence, these two methods were expected to produce the highest porosity values in this study.

Table 1: Results of porosity of the natural sample

Sample	Porosity (%) (Helium pycnometry)	Porosity (%) (Archimedes method)
Natural sample	28.1	27.74

4.2 Digital Sample Porosity

For the digital sample, porosity determination through imaging and analysis yielded a porosity value of 24.8%. It is important to acknowledge that this value is limited by various factors, including the resolution of the scanner used. This limitation means that features smaller than three times the scanner's resolution could not be clearly imaged and were hence eliminated from the final value. Additionally, the segmentation process relied on the operator's judgment, introducing the possibility of errors that could be propagated to the printed sample. The 2D slice of the sample and the grayscale distribution histogram are shown in Fig. 1. Furthermore, since the primary objective was to print a sample that would offer the same flow paths as the natural sample, only effective porosity was considered for printing. These factors collectively explain why the digital sample exhibited a lower porosity compared to the natural sample.

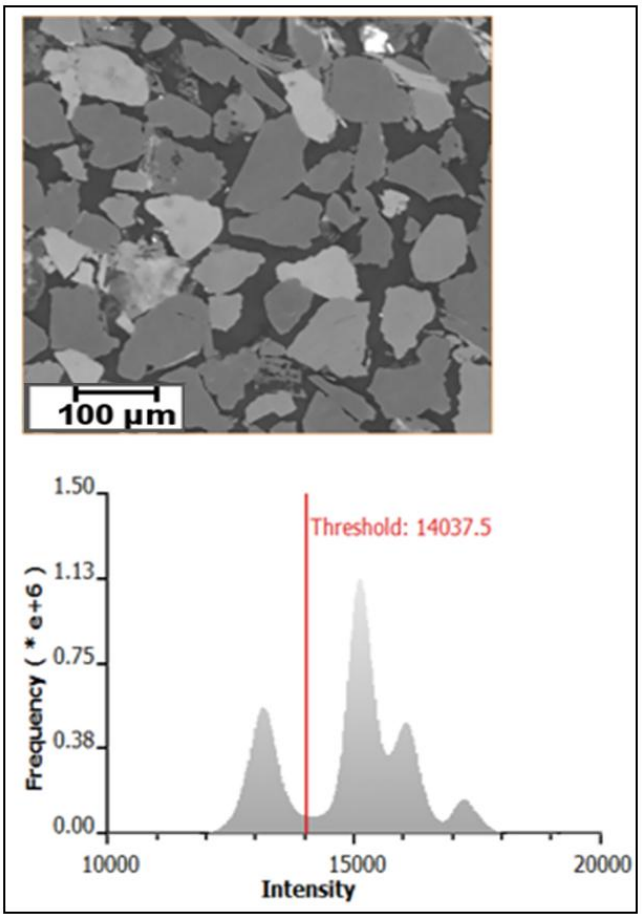

Figure 1: The 2D slice of the sample and the respective grayscale histogram showing the threshold for segmentation

4.3 Artificial Sample

The 3D model of the digital sample prepared for printing and the artificial printed sample are shown in Fig. 2. The mass of the printed sample was 1164.45 g. skeletal density was 7.7175 g.cm-3. Different porosity measurement techniques were used for the artificial sample, resulting in varying results based on the volume measured. The water displacement, Vernier caliper, 3D scanner, and theoretical methods were used to determine the sample volume, resulting in porosity values of 19.85%, 19.84%, 16.53%, and 19.59%, respectively. Detailed data are presented in Table 2.

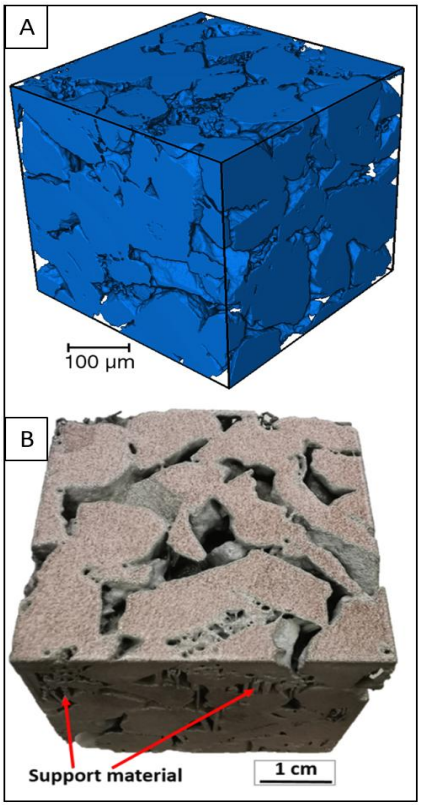

Figure 2: The 3D model of the sample prepared for printing (A) and the artificial printed sample (B) showing some visible support structures.

Table 2. Bulk Volume, Bulk Density, and measured Porosity

Method	Volume (cm3)	Bulk density	Measured porosity
Water displacement	188.25	7.57	19.85
Vernier caliper	188.23	6.19	19.84
3D Scanner	180.79	6.44	16.53
Micro-CT theoretical Vol.	187.64	6.21	19.59

4.4. Enhanced Comparison of Porosity Values and Implications

The porosity values of natural, digital, and 3D-printed sandstone samples are closely examined, as presented in Fig. 3. The digital sample's porosity was determined to approximately 25%. In the case of the 3D-printed sample, the porosity ranged from about 16.5% to about 19.9% subject to the porosity determination method applied as shown in table 2. For instance, the 3D scanning method produced the lowest porosity value. The presence of an uneven sample surface in the printed version explained this. Surface pores were perceived as surface imperfections by the scanner, which treated them as non-porous features (Kumar. 2011). As a result, the measured volume was smaller than the real volume, resulting in an underestimation of porosity. Broadly, the porosity variation between the digital and the artificial sample is primarily linked to the presence of the support structures as well

as the complexities of the 3D printing process involving Selective Laser Melting (SLM). Factors influencing this include layer thickness, laser precision, and the properties of the metal powder. Using the 3D printer's software algorithms, we determined that approximately 7% of the total volume of the 3D-printed samples was occupied by support material.

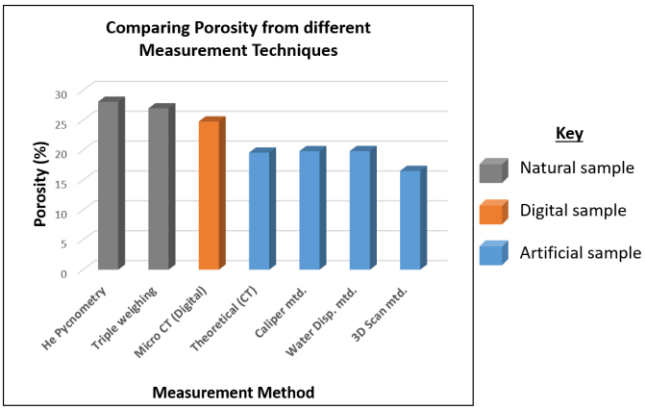

Figure 3: Comparison of porosity values between natural, digital, and artificial samples

By recalculating the porosity of the 3D-printed samples to account for the removal of this support material, we find an adjusted porosity range. If we consider the support material volume as void and add it to the total void volume, the adjusted porosity value is theoretically closer to the 25% porosity of the digital sample. This adjustment highlights the effectiveness of our 3D printing method in replicating sandstone porosity, although slight variations are present due to inherent limitations and challenges in 3D printing technology.

4.5 Comparative Analysis and Implications for Geothermal Reservoir Simulations

In our study on replicating Late Miocene sandstone porosity for geothermal energy applications, we align with the broader advancements in 3D printing technology in geosciences. Our use of Selective Laser Melting (SLM) is informed by the work of pioneers like Chia & Wu (2015) and Ishutov et al. (2021), who have laid the groundwork in precision and scalability in 3D printing. Comparative studies by Li et al. (2021) and Ishutov et al. (2015) further illustrate the evolving capabilities of these technologies in reproducing geological structures, a key focus of our research.

Our application of SLM technology marks an advancement in this field. We sought to achieve a high degree of accuracy in replicating complex sandstone porosity, crucial for understanding geothermal systems. However, this advanced approach brought to light certain challenges. Notably, there were discrepancies in porosity between our 3D-printed samples and their natural counterparts. These differences, influenced by support structures, trapped powder and printing parameters, echo the findings in the wider geoscience community, especially as seen in the work of Gomez et al. (2018) and Ibrahim et al. (2021). These researchers explored the mechanical behavior and permeability of 3D-printed sandstone analogues, shedding light on the complexities involved in 3D printing and simulation.

The synthesis of our study with these scholarly contributions highlights the importance of ongoing advancements in 3D printing technology for geothermal reservoir simulations. Addressing the challenges identified in our research is critical for the continued development of this field. This would call for advanced post processing procedures that will ensure removal of the support material from the final product. By ensuring that 3D-printed geological models are both technologically advanced and scientifically reliable, our work contributes to the understanding and exploration of geothermal energy resources. This approach not only aligns with the current technological trends but also paves the way for future innovations in geosciences.

Conclusions, Recommendations & Outlook

Conclusion

This study strategically addresses key limitations in 3D printing technology for replicating sandstone porosity. This study focuses on improving the accuracy of porosity replication by overcoming the challenges associated with achieving the desired porosity and grain size distribution, optimizing post-processing to remove support material, exploring alternative molding materials such as silica sand to better mimic the behavior of natural sandstone, and improving resolution and accuracy in 3D printing. This study also emphasizes the need to improve the reproducibility of artificial samples for cost-effective and repeatable laboratory experiments. By overcoming these important obstacles, this research aims to contribute to the advancement of 3D printing methods, making artificial sandstone samples more reliable and applicable for geothermal research in the laboratory.

Evaluation of the successes and challenges of the 3D printing process is crucial in determining the feasibility of using the artificial sample for laboratory geothermal water flooding experiments. The process has demonstrated significant successes, including the ability to accurately reproduce sandstone porosity with >79% accuracy. The proposed methodology offers a cost-effective and efficient method to create artificial sandstone samples for laboratory experiments, overcoming the high costs associated with obtaining natural samples. In addition, the reproducibility of artificial samples allows for repeated experiments, especially in cases where samples are destroyed after a single use. In laboratory flooding tests to simulate reinjection of geothermal water, repeated experiments must be conducted, but the samples cannot be reused. This explains the need for reproducible samples at a more environment friendly and faster method without having to go through the expensive drilling process.

Nevertheless, challenges still exist in the 3D printing process. These challenges include; ensuring proper post-processing and removal of support materials as well as trapped powder. These challenges need to be addressed to further improve the 3D printing process and increase the reliability of artificial samples. A viable solution would be to use different material for the support to make it easier to clean the support material from the printed geometry.

The suitability of the artificial sample for laboratory geothermal water flooding experiments depends on its ability to accurately mimic the flow behavior of natural sandstone. Considering that the artificial sample was printed on stainless steel, its mechanical properties, such as strength, stiffness, and toughness, are significantly different from those of natural sandstone. Therefore, exploring alternative printing materials, such as silica sand, that can better mimic the behavior of sandstone would provide a more suitable sample and yield valuable insights for geothermal research. Furthermore, we managed to achieve the desired porosity and grain size distribution although not at the digital model scale.

Overall, the 3D printing process has shown promise in replicating sandstone porosity and offers potential benefits in terms of cost-effectiveness and reproducibility. Further advances in the printing process, including material selection and post-processing techniques, will increase the reliability and applicability of artificial samples for geothermal water reinjection simulations.

Recommendations for Further Research

Based on the findings and limitations of this study, future research directions include exploring the use of different materials for printing, improving post-processing methods, and utilizing higher-resolution printers to achieve a more accurate sandstone grain and pore size distribution. In addition, alternative manufacturing methods, such as sand compaction with calcium carbonate cement, will be considered for the continuation of this work.

Outlook

This work is an ongoing PhD project, dealing with the physical clogging of geothermal reservoirs in the Pannonian Basin, Hungary. The knowledge gained from this study will be used for the development of a new methodology for manufacturing artificial samples that mimic the Late Miocene sandstone for repeated laboratory flooding experiments to investigate physical clogging under controlled environmental conditions. This will support the promotion of the sustainable development of geothermal energy.

Acknowledgments

We thank Dr. Ferenc Fedor and Péter Ács from Geochem Ltd., Hungary, for their assistance with sample preparation and porosity measurements. We are also grateful to the University of Szeged, especially the Department of Mineralogy, Geochemistry and Petrology, and the 3D Centre, for providing the natural sample and printing the artificial sample respectively. Portions of this work were presented at the European Geothermal PhD Days in Aachen, Germany, and Glasgow, Scotland, in 2022 and 2023.

REFERENCES

Abdallah, M., Magaldi, D., Hijazi, A., Graff, B., Dumur, F., Fouassier, J. P., Bui, T. T., Goubard, F., & Lalevée, J. (2019). Development of new high-performance visible light photoinitiators based on carbazole scaffold and their applications in 3d printing and photocomposite synthesis. *Journal of Polymer Science, Part A: Polymer Chemistry*, *57*(20), 2081–2092. https://doi.org/10.1002/pola.29471

Abutaha, S. M., Geiger, J., Gulyás, S., & Fedor, F. (2021). Assessing the representative elementary volume of rock types by X-ray computed tomography (CT)-a simple approach to demonstrate the heterogeneity of the Boda Claystone Formation in Hungary. *Geologos*, *27*(3), 157–172. https://doi.org/10.2478/logos-2021-0018

Almetwally, A. G., & Jabbari, H. (2021). 3D-Printing Replication of Porous Media for Lab-Scale Characterization Research. *ACS Omega*, *6*(4), 2655–2664. https://doi.org/10.1021/acsomega.0c04825

Angumba, P., Cárdenas, A., & Icaza, D. (2022). Geothermal and Solar Energy Applied to Air Conditioning and Electricity Generation for Homes: Case study Baños in Cuenca-Ecuador. *10th International Conference on Smart Grid (icSmartGrid), Istanbul, Turkey, 2022, pp. 407-413,* https://doi.org/10.1109/icSmartGrid55722.2022.9848548

Arandjelovic, O., X. Y., W. D., & L. I. (2015). (2015). Nondestructive high-resolution microCT scanning of small animals. Journal of Visualized Experiments,. *Journal of Visualized Experiments. (98), E52722. Https://Doi.Org/10.3791/52722*

Avizo software. (2019). Thermo Fisher Scientific, Waltham, MA, USA *https://www.fei.com/software/amira-avizo/*

Békési, E., Fokker, P. A., Candela, T., Szanyi, J., & van Wees, J. D. (2022). Ground motions induced by pore pressure changes at the Szentes geothermal area, SE Hungary. *Geothermal Energy*, 10(1). https://doi.org/10.1186/s40517-022-00214-6

Byrtus, R., Hercik, R., Dohnal, J., Martinkauppi, J. B., Rauta, T., & Koziorek, J. (2022). Low-power Renewable Possibilities for Geothermal IoT Monitoring Systems. *11th IEEE International Conference on Renewable Energy Research and Applications, ICRERA 2022*, 164–168. https://doi.org/10.1109/ICRERA55966.2022.9922835

Chia, H. N. and Wu, B. M. (2015). Recent advances in 3d printing of biomaterials. Journal of Biological Engineering, 9(1). https://doi.org/10.1186/s13036-015-0001-4

Dragonfly software. (2021). *Dragonfly software*. (Version 2021 Object Research Systems, Montreal, Canada). (Http://Www.Theobjects.Com/Dragonfly/)

Emanuel, A., Alameda, G., Behrens, R., & Hewett, T. (1989). Reservoir performance prediction methods based on fractal geostatistics. *SPE Reservoir Engineering*, 4(03), 311-318. https://doi.org/10.2118/16971-pa

Filinich, R. and Chibey, T. J. (2020). Becoming and individuation on the encounter between technical apparatus and natural system. *M/C Journal*, 23(4). https://doi.org/10.5204/mcj.1651

Földes, T., Árgyelán, G. B., Bogner, P., Romics, I., Kiss, B., & Hips, K. (2004). Application of medical computer tomograph measurements to 3d reservoir characterization. *Acta Geologica Hungarica*, 47(1), 63-73. https://doi.org/10.1556/ageol.47.2004.1.5

Gomez, J. S., Chalaturnyk, R. J., & Zambrano-Narvaez, G. (2018). Experimental Investigation of the Mechanical Behavior and Permeability of 3D Printed Sandstone Analogues Under Triaxial Conditions. *Transport in Porous Media*, *129*(2), 541–557. https://doi.org/10.1007/s11242-018-1177-0

Gunnlaugsson, E., Ármannsson, H., Thorhallsson, S., & Steingrímsson, B. (2014). Problems in geothermal operation–scaling and corrosion. *Geothermal Training Program, United Nations University*, 1-18.

Harrouz, A., Temmam, A., & Abbes, M. (2018). Renewable energy in algeria and energy management systems. *International Journal of Smart Grid.* https://doi.org/10.20508/ijsmartgrid.v2i1.10.g9

Hodder, K. J., Sanchez-Barra, A. J., Ishutov, S., Zambrano-Narvaez, G., & Chalaturnyk, R. J. (2022). Increasing Density of 3D-Printed Sandstone through Compaction. *Energies*, *15*(5). https://doi.org/10.3390/en15051813

Ibrahim, E. R., Jouini, M., Bouchaala, F., & Gomes, J. (2021). Simulation and validation of porosity and permeability of synthetic and real rock models using three-dimensional printing and digital rock physics. *ACS Omega*, 6(47), 31775-31781. https://doi.org/10.1021/acsomega.1c04429

Ilyas, S. Z., Hassan, A., & Mufti, H. (2021). Review of the renewable energy status and prospects in Pakistan. *International Journal of Smart Grid*, *5*(4), 167-173.

Ishutov, S., Hasiuk, F. J., Harding, C., & Gray, J. N. (2015). 3D printing sandstone porosity models. *Interpretation*, *3*(3), SX49–SX61. https://doi.org/10.1190/INT-2014-0266.1

Ishutov, S., Hodder, K., Chalaturnyk, R., & Zambrano-Narváez, G. (2021). A 3D printing short course: a case study for applications in the geoscience teaching and communication for specialists and non-experts. *Frontiers in Earth Science*, 9. https://doi.org/10.3389/feart.2021.601530

Jakus, A. E., Geisendorfer, N. R., Lewis, P. L., & Shah, R. N. (2018). 3D-printing porosity: A new approach to creating elevated porosity materials and structures. *Acta Biomaterialia*, *72*, 94–109. https://doi.org/10.1016/j.actbio.2018.03.039

Jennings, J. W., Lucia, F. J., Ruppel, S. C., John, A., & Katherine, G. (2002). 3D modeling of stratigraphically controlled petrophysical variability in the south wasson clear fork reservoir. *The SPE Annual Technical Conference and Exhibition, San Antonio, Texas, SPE*. https://doi.org/10.2118/77592-ms

Kim, J. S., Shim, G. S., Baek, D., Back, J. H., Jang, S. W., Kim, H. J., … & Yeom, J. S. (2019). Uv/uv step-curing of optically clear acrylate adhesives for mobile devices. *Express Polymer Letters*, 13(9), 794-805. https://doi.org/10.3144/expresspolymlett.2019.68

Kumar, J., Abulrub, A. H. G., Attridge, A., & Williams, M. A. (2012). Effect of X-ray computed tomography scanning parameters on the estimated porosity of foam specimens. *Applied Mechanics and Materials*, *110*, 808-815.

Koroncz, P., Vizhányó, Z., Farkas, M. P., Kuncz, M., Ács, P., Kocsis, G., Mucsi, P., Fedorné Szász, A., Fedor, F., & Kovács, J. (2022). Experimental Rock Characterisation of Upper Pannonian Sandstones from Szentes Geothermal Field, Hungary. *Energies*, *15*(23). https://doi.org/10.3390/en15239136

Lee, Hae Ok, and John P. Heller. (1990). Laboratory Measurements of CO_2-Foam Mobility. *SPE Res Eng* 5: 193–197. https://doi.org/10.2118/17363-PA

Li, A., Zhang, S., Xu, C., Zhao, X., & Zhang, X. (2021). 3D Printing of True Pore-Scale Berea Sandstone and Digital Rock Verification. *SPE Journal*, *26*(6), 3719–3724. https://doi.org/10.2118/205383-PA

Qasim, M., Haq, F., Kang, M. H., & Kim, J. H. (2019). 3D printing approaches for cardiac tissue engineering and role of immune modulation in tissue regeneration. In *International Journal of Nanomedicine* (Vol. 14, pp. 1311–1333). Dove Medical Press Ltd. https://doi.org/10.2147/IJN.S189587

Saptadji, N. M. (2001). *Teknik panasbumi* (1st ed.). Penerbit ITB.

Shayan, M. E., Najafi, G., & Nazari, A. (2021). The biomass supply chain network auto-regressive moving average algorithm. *International Journal of Smart Grid*. https://doi.org/10.20508/ijsmartgrid.v5i1.153.g135

Siregar, E. , A. H. , & M. M. (2020). The importance of porosity and permeability measurement for geothermal reservoir characterization. *Journal of Physics: Conference Series, 1567, 012017.* Https://Doi.Org/10.1088/1742-6596/1567/1/012017

Sofyan, A., Dwi, Y., Bujang, G., and Dewi, D. C. (2023). Analysis of the Z Well Production Test Using the Horizontal LIP Pressure Method at PT. Pertamina Geothermal Energy Ulubelu Area." *Indonesian Journal of Energy and Mineral*, 3(1), 40–55

Sofyan A, S. J. S. A. H. (2024). Investigation of Zone and Type of Scaling Based on the Fluid Flow Pattern in the Geothermal Well "X" at the Salak Geothermal Field - Indonesia. *International Journal of Renewable Energy Research, 14*(1).

Sofyan, A., Wiharti, S., Szanyi, J., Suranta, B. Y., and Njeru, R. (2023). Determination of Scaling Zone and Scaling Type in Slotted Liner Based on the Fluid Flow Pattern in the Geothermal Well

'X.' *International Journal of Renewable Energy Research*, 13(1), 276–286. https://doi.org/10.20508/ijrer.v13i1.13603.g8681

Tamir, T. S., Xiong, G., Jiang, J., Shen, Z., Lodhi, E., Ali, H., & Wan, L. (2022). Terms Development of Additive Manufacturing. *2022 IEEE 2nd International Conference on Digital Twins and Parallel Intelligence, DTPI 2022*. https://doi.org/10.1109/DTPI55838.2022.9998939

Toth, A., (2020). Country Update for Hungary. *World Geothermal Congress 2020* www.mbfsz.gov.hu

Wang, G., Song, L., Wang, Q., Tian, Z., Fan, J., Wang, Y., … & Shen, H. (2022). Experimental study on the mechanical properties, acoustic emission characteristics, and permeability evolution of sandstone under triaxial hydromechanical coupling. *Energy Science & Engineering*, 10(12), 4466-4480. https://doi.org/10.1002/ese3.1281

Willems, C., Cheng, C., Watson, S., Minto, J., Williams, A., Walls, D., … & Westaway, R. (2021). Permeability and mineralogy of the újfalu formation, hungary, from production tests and experimental rock characterization: implications for geothermal heat projects. *Energies*, 14(14), 4332. https://doi.org/10.3390/en14144332

Wu, H., Ju, Y., Han, X., Ren, Z., Sun, Y., Zhang, Y., & Han, T. (2022a). Size effects in the uniaxial compressive properties of 3D printed models of rocks: an experimental investigation. *International Journal of Coal Science and Technology*, *9*(1). https://doi.org/10.1007/s40789-022-00556-3

Xie, H., Basu, S., & DeMeter, E. C. (2021). Coupling monte carlo light propagation method and curing kinetic equations to model the degree of conversion evolution of uv-curable composites. *Industrial & Engineering Chemistry Research*, 60(28), 10431-10444. https://doi.org/10.1021/acs.iecr.1c01585

Yudha SW, Tjahjono B, Longhurst P. (2022). Unearthing the dynamics of Indonesia's geothermal energy development. *Energies*, 15(14), 5009. https://doi.org/10.3390/en15145009

Zhang, Z., Kruschwitz, S., Weller, A., & Halisch, M. (2018). Enhanced pore space analysis by use of μ-CT, MIP, NMR, and SIP. *Solid Earth*, 9(6), 1225–1238. https://doi.org/10.5194/se-9-1225-2018